Title

Electrospun PGS:PCL Microfibers Align Human Valvular Interstitial Cells and Provide Tunable Scaffold Anisotropy

Journal

Advanced Healthcare Materials, 3(6)

ISSN

2192-2640

Authors

Masoumi, Nafiseh
Larson, Benjamin L
Annabi, Nasim
et al.

Publication Date

2014-06-01

DOI

10.1002/adhm.201300505

Peer reviewed

Electrospun PGS:PCL Microfibers Align Human Valvular Interstitial Cells and Provide Tunable Scaffold Anisotropy

Nafiseh Masoumi, Benjamin L. Larson, Nasim Annabi, Mahshid Kharaziha, Behnam Zamanian, Kayle S. Shapero, Alexander T. Cubberley, Gulden Camci-Unal, Keefe. B. Manning, John E. Mayer Jr., and Ali Khademhosseini**

Tissue engineered heart valves (TEHV) can be useful in the repair of congenital or acquired valvular diseases due to their potential for growth and remodeling. The development of biomimetic scaffolds is a major challenge in heart valve tissue engineering. One of the most important structural characteristics of mature heart valve leaflets is their intrinsic anisotropy, which is derived from the microstructure of aligned collagen fibers in the extracellular matrix (ECM). In the present study, a directional electrospinning technique is used to fabricate fibrous poly(glycerol sebacate):poly(caprolactone) (PGS:PCL) scaffolds containing aligned fibers, which resemble native heart valve leaflet ECM networks. In addition, the anisotropic mechanical characteristics of fabricated scaffolds are tuned by changing the ratio of PGS:PCL to mimic the native heart valve's mechanical properties. Primary human valvular interstitial cells (VICs) attach and align along the anisotropic axes of all PGS:PCL scaffolds with various mechanical properties. The cells are also biochemically active in producing heart-valve-associated collagen, vimentin, and smooth muscle actin as determined by gene expression. The fibrous PGS:PCL scaffolds seeded with human VICs mimick the structure and mechanical properties of native valve leaflet tissues and would potentially be suitable for the replacement of heart valves in diverse patient populations.

1. Introduction

There are five million patients diagnosed with heart valve diseases every year in the United States as reported by the American Heart Association. Heart valve operations are performed on approximately 300 000 patients annually in the United States.[1,2] For many patients, the diseased heart valves are replaced by mechanical or bioprosthetic heart valves through surgery.[2] However, valve replacement devices have limitations including the possibility of long-term mechanical failure and lack of biocompatibility.[1–4] In addition, most heart valve replacements are not suitable for pediatric patients whose heart valves are actively growing. Tissue engineering has emerged as a promising approach to create functional heart valves that can integrate with the native tissues and offer the potential for growth and remodeling.[1,2,5]

One tissue engineering approach to creating heart valves uses scaffolds as temporary supports. To engineer functional heart valve leaflets, the scaffolds should: a) mimic the anisotropic mechanical properties and elasticity of native heart valve leaflets,[6,7] b) have a fibrous structure containing aligned fibers, resembling the microstructure of the native tissue,[8,9] c) have elastic deformation similar to native tissues,[10,11] and d) possess controlled degradation and support tissue regeneration at a rate to maintain structural

N. Masoumi, Dr. B. L. Larson, Dr. N. Annabi, Dr. M. Kharaziha, B. Zamanian, Dr. G. Camci-Unal, Prof. A. Khademhosseini
Harvard-MIT Division of Health Sciences and Technology
Massachusetts Institute of Technology
65 Landsdowne Street, Cambridge, MA 02139, USA
E-mail: alik@rics.bwh.harvard.edu

N. Masoumi, Dr. N. Annabi, Dr. M. Kharaziha, B. Zamanian, Dr. G. Camci-Unal, Prof. A. Khademhosseini
Center for Biomedical Engineering
Department of Medicine, Brigham and Women's Hospital
Harvard Medical School
75 Francis Street, MA 02115, USA

N. Masoumi, Dr. K. S. Shapero, A. T. Cubberley, Prof. J. E. Mayer Jr.
Department of Cardiac Surgery
Boston Children's Hospital
Harvard Medical School
300 Longwood Avenue, Boston, MA 02115, USA
E-mail: john.mayer@cardio.chboston.org

N. Masoumi, Prof. K. B. Manning
Department of Bioengineering
The Pennsylvania State University
205 Hallowell Building, State College, PA 16801, USA

Dr. B. L. Larson
The David Koch Institute for Integrative Cancer Research
Massachusetts Institute of Technology
500 Main Street, Cambridge, MA 02139, USA

Dr. N. Annabi, Prof. A. Khademhosseini
Wyss Institute for Biologically Inspired Engineering
Harvard University
3 Blackfan Circle, Boston, MA 02115, USA

DOI: 10.1002/adhm.201300505

integrity.[1,12] Previously fabricated scaffolds for tissue engineered heart valve (TEHV) have had some limitations including plastic deformation,[13] high stiffness (e.g., non-woven scaffolds),[14–16] non-anisotropic properties (e.g., homogeneous structural–mechanical properties in fibrin gels),[17,18] low stability, and lack of suturability (e.g., hydrogel-based scaffolds).[19,20]

The functionality of heart valve tissue is derived from its complex architecture. Recently, significant attempts have been made to recapitulate this complexity in vitro while providing a suitable environment for cell proliferation and ECM production.[6,12,20,21] Several of these studies have fabricated scaffolds for TEHV by using synthetic materials. For example, Gottlieb et al. used non-woven scaffolds composed of polyglycolic acid (PGA) and poly-L-lactic acid (PLLA) as TEHV. Despite promising results in vitro, these scaffolds stiffened in vivo over time.[22,23] In another study, Masoumi et al. generated highly elastic microfabricated poly(glycerol sebacate) (PGS) scaffolds for TEHV. The fabricated elastomers had an anisotropy and elastic modulus similar to native pulmonary heart valves (≈4 MPa). However, the application of microfabricated PGS scaffolds for TEHV were limited by their non-fibrous structures and the absence of interconnected micropores within 3D constructs to support tissue formation.[6,21]

Our group recently fabricated elastic fibrous scaffolds containing random fibers by electrospinning PGS and poly(caprolactone)(PCL) to produce TEHV constructs.[12,13] The fabricated electrospun PGS/PCL scaffold had an elastic modulus in the range of 8.5 MPa that mimicked the mechanical stiffness of the native heart valve.[13] In addition, these composites supported the attachment and growth of porcine valvular interstitial cells (VICs) and increased the production of collagen compared to pure PCL.[12] However, these scaffolds were unable to simulate the anisotropic characteristics of the native heart valve.

In addition to the fabrication of suitable TEHV scaffolds, the use of appropriate cell types may play an important role in heart valve regeneration. VICs have been used for engineering heart valves due to their presumed ability to synthesize appropriate ECM.[6,12] However, in previous studies, nonhuman VICs have been used, which other studies have shown, can differ from human VICs in phenotypic and biochemical responses.[13,24] Therefore, it is important to study the interaction of human VICs and biomaterials when designing scaffolds for clinical applications.

In this study, we aimed to fabricate elastic PGS:PCL scaffolds using directional electrospinning to induce human aortic VICs proliferation and maturation. We hypothesized that PGS:PCL scaffolds containing aligned fibers could provide anisotropic mechanical properties similar to native heart valves. The engineered composites are expected to provide biocompatibility, durability, and biodegradability. The tunable mechanical properties of fabricated PGS:PCL scaffolds provide the ability to mimic heart valve leaflets with various mechanical properties. The capability of fabricated composites to support viability, attachment, proliferation, and protein expression of aortic human and porcine VICs was assessed.

2. Results and Discussion

In this study, directional electrospinning was used to fabricate scaffolds with aligned fibers, which enhanced mechanical properties of anisotropy. As the anisotropic mechanical characteristics of heart valves primarily rely on the microstructure of aligned collagen fibers existing in each layer of the heart valve leaflets,[11,25] it is necessary to study and understand cellular behavior and function on the engineered scaffolds, to assess the degree to which the anisotropic fibrous structure of native tissue is reproduced.

2.1. PGS:PCL Scaffold Structure and Mechanics

PGS has shown promising biological characteristics for supporting VICs yet its mechanical strength cannot withstand the pressures in the heart valve.[6] As a result, combining PGS with another biocompatible synthetic polymer with higher mechanical properties can be an alternative approach for engineering heart valve scaffolds.[12] Previously, our lab used electrospinning to develop PGS:PCL composite scaffolds with tunable stiffness. This process does not require post-processing (photocrosslinking or thermal curing) as opposed to other PGS blended fibrous scaffold fabrication techniques such as photopolymerizing acrylated PGS[26,27] and coaxial electrospinning of PGS/PLLA blends.[28] However, the fabricated PGS:PCL constructs were minimally elastic (less than 5%) and non-anisotropic.[12,13] In this study, we modified the fabrication technique to create PGS:PCL scaffolds with anisotropic characteristics and enhanced mechanical properties while maintaining cell functionality. It is expected that both the microstructure and mechanical properties of engineered scaffolds, resembling the native heart tissue, affect cellular behavior.

2.1.1. Fabrication and Chemical Characterization of Microfibrous PGS:PCL Scaffolds

Our composite materials contained PGS, which facilitated cell attachment and growth, and PCL, which provided mechanical support. Random or aligned fibers were fabricated by using different electrospinning collectors (**Figure 1**A). To align fibers, two parallel aluminum electrodes bordering a Teflon sheet collector were employed, whereas random fibers were produced on an aluminum electrode plate. We fabricated electrospun PGS:PCL scaffolds at various ratios of PGS and PCL including 2:1,1:1, 1:2, and 1:4. The chemical characterization of these compositions, as well as PGS pre-polymer, and pure PCL were assessed using FTIR analysis (Figure 1B,C). Two primary bands were detected at 1726 cm^{-1} (stretching vibrations of the carboxyl (C =O)) and 1180 cm^{-1} (stretching vibrations of the ether groups (C—O)) in the PCL spectrum. Other bands such as C—O stretching vibrations at 1050 cm^{-1}, symmetric C—H stretching at 2865 cm^{-1}, and C—O and C—C stretching at 1296 cm^{-1} were observed in the spectrum corresponding to PCL.[29] The PGS pre-polymer spectrum consisted of methylene groups (C—H) at 2933, 2908, and 1390 cm^{-1}. The ester band was present at stretching vibration C—O bonds at 1173 cm^{-1}, and the strong carbonyl stretching bonds (C—O) at 1732 cm^{-1} were also exhibited in the spectrum along with the weak absorption bonds at 930 and 1300 cm^{-1} confirming the presence of aliphatic acid (sebacic acid) in the polymer.[30,31] All of the characteristic bands of PGS are overlapped with PCL bands with the exception of a peak at 1228 cm^{-1} ascribed to C—O groups. Hydroxyl

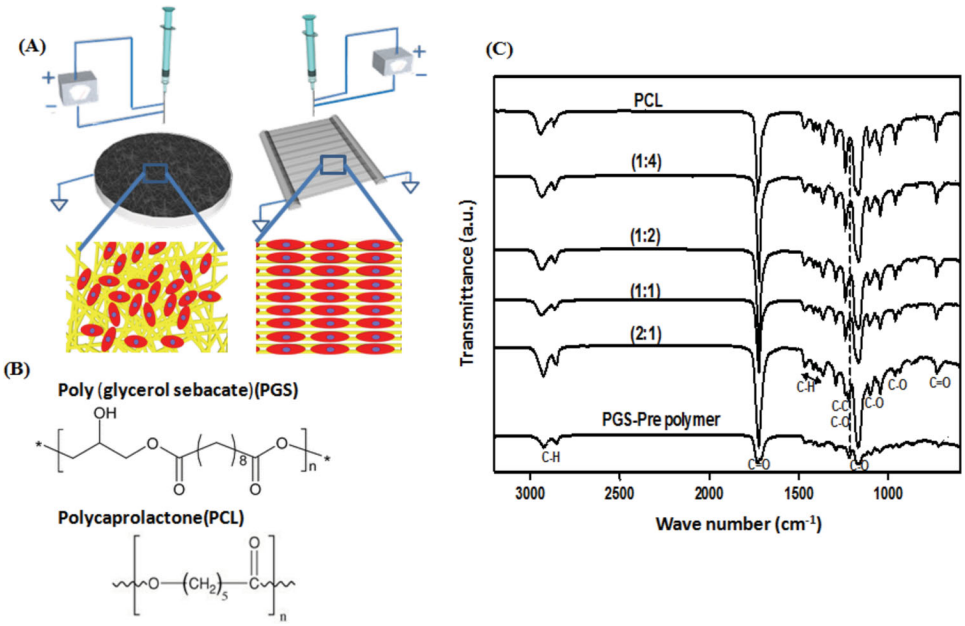

Figure 1. Schematic diagram of scaffold fabrication process and polymer composition. A) Two electrospinning techniques were used to design the scaffolds with random and aligned fibers. The random fibers were collected on a cylindrical metal plate and aligned fibers were collected between two aluminum electrodes. The randomly deposited fibers resulted in a random cellular orientation and aligned fibers resulted in cell alignment. B) Molecular structure of PGS and PCL representing the ester bonds and alkaline groups. C) FTIR spectra of the fibrous scaffolds with different ratios of PGS:PCL (2:1, 1:1,1:2, and 1:4) compared with pure PCL and pure PGS sheets.

groups were present at approximately 3200–3500 cm^{-1} but were overshadowed by the amplitude of the much larger peaks present in the spectrum. Though the different polymer compositions grant different mechanical features, described later, their chemical properties do not differ considerably even after brief immersion in NaOH to promote scaffold hydrophilicity prior to in vitro tests.

2.1.2. Physical Characteristics of PGS-PCL Scaffolds

The porosity of scaffolds has a critical role in cell–cell and cell–matrix interactions. The presence of pores facilitates oxygen and media diffusion throughout the scaffold and provides an increased surface area for cell attachment.[32,33] The pore sizes of aligned and random fiber scaffolds were measured by SEM and compared for different combinations of PGS:PCL (**Figure 2**A–D). The aligned fiber scaffolds with higher concentrations of PGS had lower viscosity and fewer polymer chain tangles. This surface tension affected the processing and resulted in beads and spindles[13,34] and less aligned fibers in the 2:1 polymer ratio (Figure 2A). As the PGS:PCL ratio decreased, the pore size increased in the aligned fiber scaffolds (Figure 2C). In addition, there was a two-fold increase in the aligned fibers' size with increasing PCL concentration, that could be due to the larger relative molecular size of PCL compared to PGS (Figure 2D).

Engineered composite heart valve replacements should ideally provide temporary mechanical support while allowing for the generation of new ECM by the transplanted and host cells. To allow for the growth and remodeling of the fabricated valves by VICs and surrounding tissue, the scaffold is required to degrade at predictable loss rates.[1,12] The degradation of aligned fibers was studied as a function of bulk weight loss over a period of 10 days (Figure 2E). The degradation rate of the scaffolds was ratio dependent where the greater the PGS:PCL ratio the faster the degradability. These observations were in agreement with other reports where PCL had a resident time in vivo on the order of a few years whereas PGS degraded within weeks to months.[35–37] As shown in Figure 2E, the degradation rate (wet weight loss) changed from 18% for the (1:4) ratio to about 40% for the (2:1) ratio. The scaffold wettability was also tested, and indicated that all ratios of fabricated PGS:PCL scaffolds were highly hydrophilic as water drops rapidly penetrated and spread through all tested compositions, enabling facile cell seeding but precluding contact angle measurement (data not shown).

Normal leaflet opening and closure during blood flow are dependent on the anisotropic mechanical characteristics of the leaflet.[1,6] Polymers with different properties spun in a defined manner, could be employed for the replacement of these native valves if their mechanical features could be made to coincide. Here, we used uniaxial tensile testing to characterize the mechanical properties of the scaffolds under external stress. Representative stress–strain curves for all the ratios of the PGS:PCL scaffolds with random fibers were compared (**Figure 3**A). Representative stress–strain curves for the 1:1 and 1:4 PGS:PCL scaffolds tested along (PD) or perpendicular (XD) to the direction of the aligned fibers were also compared (Figure 3B). The stress–strain curves for the random fibers exhibited a small linear region followed by a significant deformation known as creep (starting from approximately 8% strain). However, for aligned fibers, less deformation and creep were

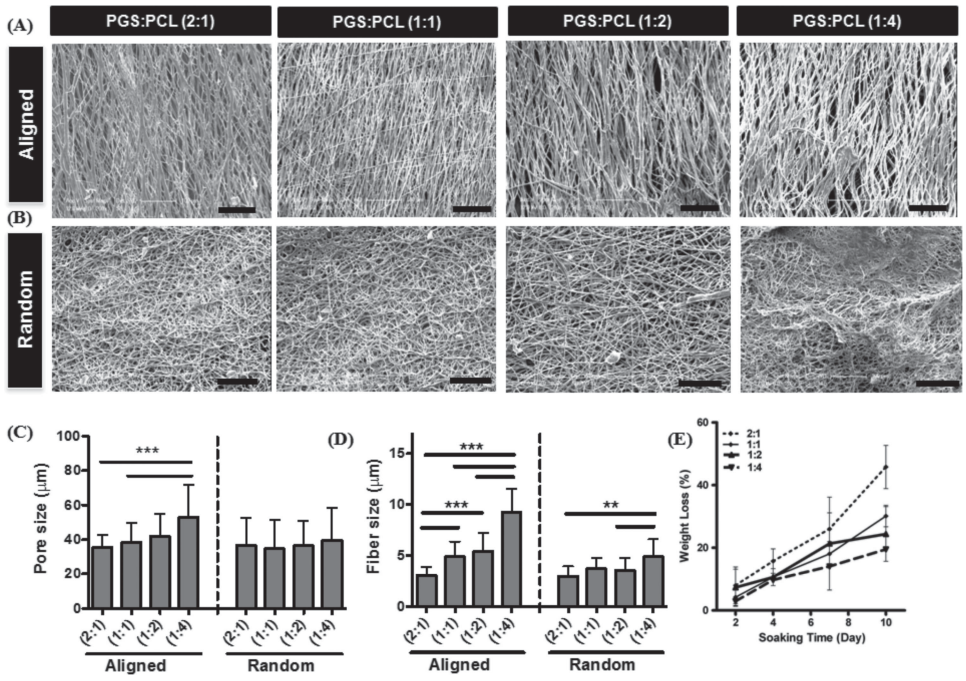

Figure 2. Scaffold fiber SEM characterization and degradation. A,B) SEM images of aligned and random fibrous scaffolds (scale bar: 100 μm). C) Pore size measurements demonstrated slightly larger pore sizes for aligned scaffolds with more PCL content. The pores in random fibers were in the same size range. D) Fiber sizes of aligned and random fibrous scaffolds were measured. Higher values were observed for the (1:4) PGS:PCL ratio aligned scaffolds compared to other ratios of aligned scaffolds. Similar trends were observed for the random fibers. E) Representative weight loss curves of scaffolds following 10 days of soaking in PBS with 0.5 M NaOH. As expected, scaffolds with higher PGS content degraded faster.

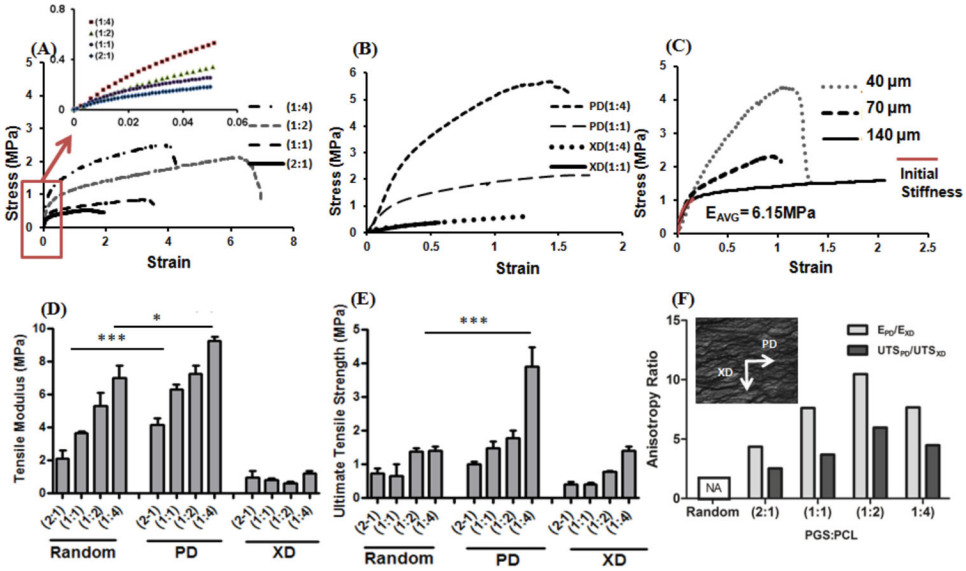

Figure 3. Uniaxial mechanical testing of unseeded scaffolds in two directions. A) Representative stress–strain curves of random scaffolds for all the ratios of the PGS:PCL scaffolds demonstrated that scaffolds with random fibers deformed extensively following 5%–10% strain. The initial stiffness and UTS increased by increasing the PCL content in polymer ratios. B) Representative stress–strain curves of aligned scaffolds for (1:1) and (1:4) ratios of the PGS:PCL shown in two directions (PD and XD). Scaffolds were stiffer in PD directions. C) Representative stress–strain curves of aligned scaffolds with different thicknesses depicted for the ratio of (2:1). Similar initial stiffnesses were observed with divergent relationships between UTS and scaffolds stiffness. As the thickness of the aligned scaffolds increased, greater deformations were observed in the stress–strain curves. This deformation was similar to that of the random fiber scaffolds. D,E) Tensile modulus and UTS were compared between random and aligned scaffolds in PD and XD direction. F) Anisotropy of scaffolds was measured for PGS-PCL scaffolds of varying ratios, which demonstrated that the values for (1:1), (1:2), and (1:4) were similar to the native tissues.

observed in the stress–strain curves, similar to the trend for an elastic material. This could be due to the structural features of aligned fibers that are oriented along the direction of the tensile load.[38] Moreover, aligned scaffolds were stiffer in the PD direction compared to XD direction, which resulted in anisotropic characteristics for these scaffolds. Interestingly, we observed a relation between the ultimate tensile strength and the thickness of scaffolds with aligned fibers as shown in Figure 3C (illustrated here with a ratio of (1:2)). While the initial stiffness of all three scaffolds with different thicknesses was similar, the ultimate tensile stresses decreased by increasing the thickness. The trend of the stress–strain curves for the thicker, aligned scaffolds resembled the same trend as scaffolds with random fibers with a large deformation region. This finding could be due to the fact that thicker scaffolds contained more random fibers due to the shielding of the polymer from the electrodes as the thickness of the scaffold increased (40 μm average thickness with UTS of 6.44 ± 1.70 MPa, 70 μm average thickness with UTS of 2.46 ± 0.66 MPa and 140 μm average thickness with UTS of 1.47 ± 0.15 MPa). As shown in Figure 3D–F, the stiffness, UTS, and anisotropic characteristics of scaffolds with aligned fibers improved (in PD direction) compared to the scaffolds with random fibers. The presence of more PCL content in the polymer solution increased the elastic modulus and ultimate strength with a lower strain to failure. Though fiber size increased with increasing PCL content in the aligned scaffolds, this phenomenon was not present in the random scaffolds. Here, we observed a step-wise increase in PD moduli with greater PCL content in both the random and aligned scaffolds, which was not dependent on the size of the fibers. Based on our results, electrospinning of PGS:PCL with the ratios ranging from (2:1) to (1:4) yielded scaffolds with anisotropic and tunable mechanical characteristics, which matched the native tissue stiffness, ultimate tensile strength, and anisotropy.[6] Mechanical properties (e.g., E, UTS, and ef) of each of the different groups of scaffolds are listed in **Table 1**.

Supporting information, Figure 1A–C data include the mechanical properties of scaffolds in wet and dry conditions. Wet scaffolds were less stiff compared to dry scaffolds. In the case of (1:4), the ultimate tensile strength was particularly disparate between the wet and dry conditions. This effect could be attributed to the absorbed water decreasing resistance to deformation, whereas in dry conditions entangled fibers had a high sliding friction between polymer chains.[39] We found that the aligned patterns enhanced the elasticity and anisotropy of the engineered scaffold, and more closely resembled the mechanical properties of the native ECM surrounding the VICs in vivo. The effect of overall polymer concentration was also evaluated (for 1:1 ratio), and we found that 20% polymer concentration used in this study had improved mechanical properties compared to 33% reported in the previous study.[13]

Table 1. Mechanical properties of aligned and random fibrous scaffolds.

Sample	Structure	Ultimate tensile strength [MPa]	Young's modulus [MPa]	Strain-to-failure
(2:1)	Random	0.73 ± 0.26	2.09 ± 0.91	2.04 ± 0.78
	PD	1.01 ± 0.16	4.16 ± 1.00	0.90 ± 0.16
	XD	0.48 ± 0.14	0.95 ± 0.68	1.67 ± 1.01
(1:1)	Random	0.86 ± 0.03	3.64 ± 0.27	4.26 ± 1.02
	PD	1.5 ± 0.55	6.31 ± 1.59	0.8 ± 0.29
	XD	0.40 ± 0.12	0.83 ± 0.16	3.29 ± 1.7
(1:2)	Random	1.3 ± 0.18	5.32 ± 1.45	2.86 ± 0.96
	PD	1.79 ± 0.41	7.28 ± 1.07	1.37 ± 0.51
	XD	0.77 ± 0.09	0.6 ± 0.19	2.57 ± 0.4
(1:4)	Random	2.21 ± 0.34	7.05 ± 1.45	4.21 ± 0.34
	PD	3.98 ± 1.18	9.28 ± 0.43	1.15 ± 0.22
	XD	0.89 ± 0.11	1.21 ± 0.33	2.69 ± 0.47

2.2. Composites Developed with PGS:PCL Scaffolds Seeded with VICs

To assess the utility of PGS:PCL scaffolds for heart valve tissue engineering, we seeded the electrospun scaffolds with primary VICs and studied the effects of scaffold stiffness and architecture on cellular growth and alignment. Though most research on TEHVs has been performed in vitro with porcine and other non-human cell sources, here we were able to employ relevant human primary cells and directly compare them with non-human cell counterparts used in other studies.[40]

Recently, more studies have been dedicated to TEHV scaffolds design,[6,20,21] culturing tissues in bioreactors,[41] and adopting appropriate cell types for clinical relevance. The complexity of heart valve physiology has received considerable attention particularly at the macroscale to observe tissue behavior.[1] However, fewer studies have focused on the biosynthesis,[42] regulation,[43] and contractile[44] characteristics of interstitial cells.[22] This is significant given the recent interest in changes imparted to tissues through the stiffnesses of substrates. This is particularly evident in the field of tissue engineering, where artificial materials over a wide range of mechanical properties are combined with dissociated primary cells.[45]

2.2.1. Cell Viability and Adhesion on Microfibrous PGS–PCL Scaffolds

For the primary assessment of the cells' interaction with scaffolds, cell attachment and viability were measured based on DAPI staining (**Figure 4**A) and live/dead assays (Figure 4B), respectively. The cells were seeded on the surface of the scaffold at a concentration of approximately 140–180 cells mm^{-2} (Figure 4C). Based on the initial cell density, these values indicated that 60–70% of the cells attached to the scaffolds. Cellular attachment was higher on the surfaces of the scaffolds treated by NaOH compared to untreated scaffolds (data not shown). In addition, the differences of cell attachment between different combinations of PGS:PCL were statistically negligible. As was expected, since the cells were not exposed to lethal polymerization conditions and directly seeded on the prefabricated scaffold, the viability was high at 85%–90% range. There was a slight decrease in cell viability during the 10 days of culture, which is typical of cells seeded on synthetic scaffolds (Figure 4D).

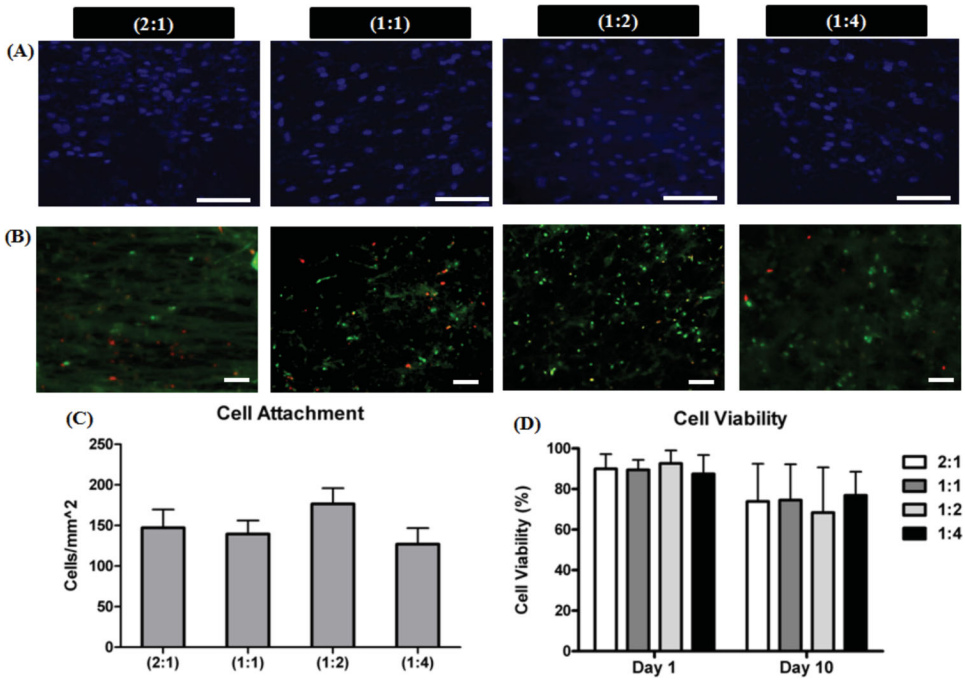

Figure 4. Human VIC attachment and viability on aligned fibrous scaffolds. A,B) Representative images of DAPI (Nuclei: blue stain) and Live/dead staining of cultured VICs on the aligned scaffolds at day 1 (Live cells: green stain, Dead cells: red stain), C) quantification of cell attachment at day 1 and D) live/dead assay results at days 1 and 10.

2.2.2. Cell Alignment Analysis

There is evidence suggesting that collagen secretion and collagen fibril formation by VICs[46] are affected by trans valvular pressure and the spatial arrangement of VICs across the circumferential direction in heart valve leaflets.[47] Previous studies have also confirmed the role of substrate topography[48,49] on fiber alignment and cell spreading.[50–52] As it is presented here, applying directional electrospinning not only enhanced the mechanical properties of PGS–PCL scaffolds but also aligned the attached cells toward the direction of fibers (**Figure 5**). Following cell alignment analysis, cells seeded on the randomly deposited PGS:PCL combinations were less than 20% aligned, whereas, cells cultured on aligned scaffolds were more than 50% aligned in the direction of the deposited fibers. The effect of substrate stiffness and structure on cell alignment is presented in Supporting Information, Figure 1F. Scaffolds that were less stiff (2:1 and 1:1 ratio) had slightly more aligned cells. This result could be due to the lower resistance of the substrate to cell arrangement and matrix formation along the fiber direction.[53] These results suggested that the scaffold structure and to a lesser degree, mechanical characteristics have effects on the human VICs morphology and organization.[38,44,45] The increase in cell alignment with higher concentrations of PGS could be due to the presence of smaller fiber diameters, which was shown to be more effective in allowing VIC attachment and alignment. Cell spreading improved on scaffolds with higher PGS concentrations at the earlier time points assayed (Supporting Information, Figure 2). F-actin images demonstrated more cell spreading on the 2:1 ratio compared with 1:4. These scaffolds were stained 12 h after seeding, though the differences were minimal at later time points and cells were mostly spread on all ratios (Figure 5A).

2.2.3. Protein Expression, Cell Proliferation, and Metabolic Activity

We used primary human VICs to evaluate various cellular behavior including proliferation, gene expression, and protein expression on PGS:PCL scaffolds with different mechanical characteristics.

Collagen Expression. In a study examining the stiffness at which VICs become activated, it was observed that VICs could be activated at stiffnesses above ≈2.5 kPa, (with or without the addition of TGFb), and in some settings, environmental stimuli (i.e., stiffness) had more of an influence on cell phenotype than chemical stimuli (i.e., TGFb).[54] **Figure 6**A depicts the collagen type I gene expression on cell seeded scaffolds, all of which were approximately one order of magnitude more stiff than those tested in the previous study.[54] We observed that more collagen was expressed by cells on the PGS:PCL composites than on the tissue culture plates, though at the ratios of (1:1) and (1:2) it was not statistically significant. The highest collagen expression occurred on scaffolds with (2:1) PGS:PCL polymer ratios.

αSMA Expression. Other studies have shown that healthy adult VICs exhibit a quiescent, fibroblast-like phenotype, expressing vimentin and, to a lesser degree, αSMA (myofibroblast marker).[55] During fetal development, active VICs are denser, proliferate more and undergo apoptosis more than in adult valves. After birth, these valve cells become more quiescent and the collagen content of the valves matures.[56] However, activated VICs have been observed in valves experiencing abnormal hemodynamic conditions.[57] These activated

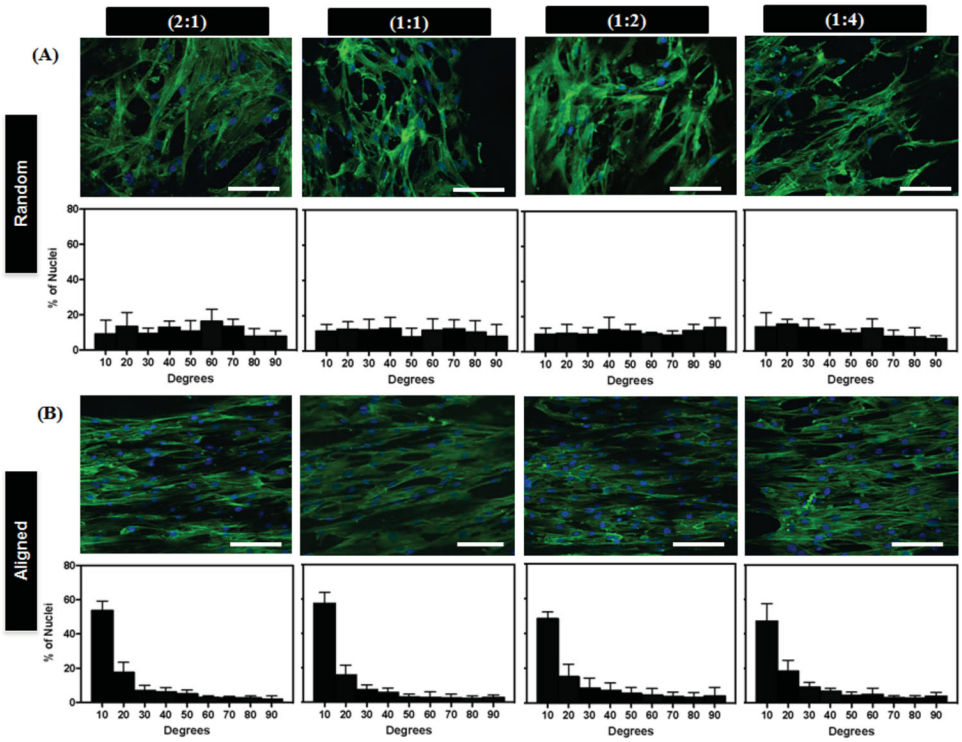

Figure 5. Human VIC alignment on fibrous scaffolds. A,B) Actin filaments and nuclei stained with Phalloidin and DAPI on random and aligned scaffolds at day 14. Bottom panels are the the alignment quantifications of VICs on the scaffolds. Cell alignment was significantly higher for the scaffolds with aligned fibers (≈50%–60% aligned cells toward the direction of fibers) (scale bar = 100 μm).

VICs (myofibroblasts) begin proliferating[58] and contribute to excessive ECM remodeling, ultimately leading to fibrosis and disease.[59,60]

Similar to the diseased phenotype, in vitro culturing can activate the VICs to transform from a quiescent, αSMA negative phenotype, to an activated myofibroblast like phenotype

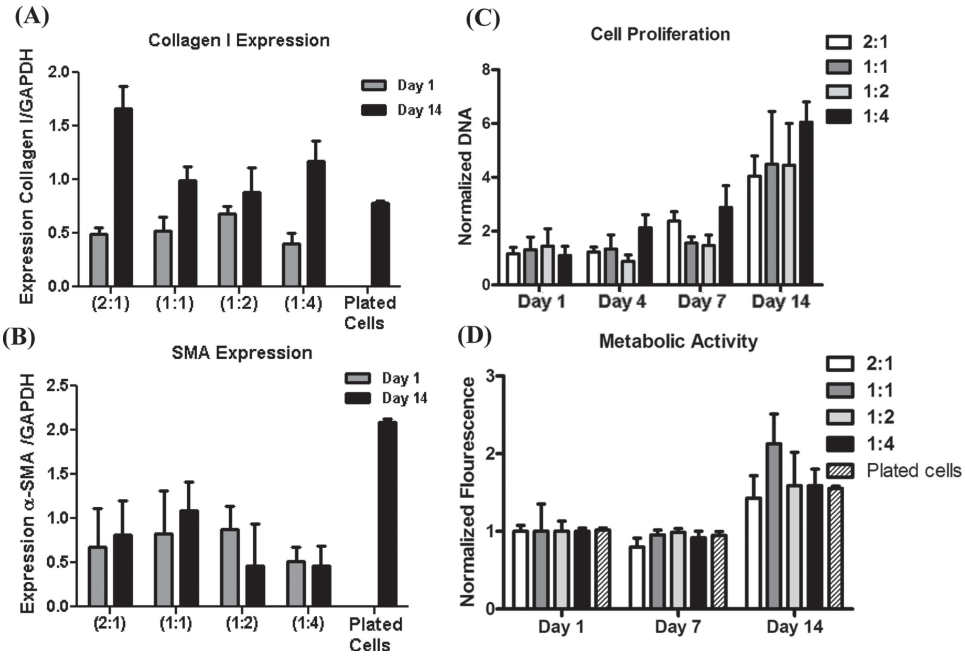

Figure 6. The effect of aligned scaffolds on human VIC gene expression, proliferation, and metabolic activity. A,B) Collagen type I and αSMA expression, as measured by PCR, for human VICs seeded on PGS–PCL scaffolds measured on days 1 and 14. Cells cultured for 14 days on tissue culture plates were used as controls. C) Cell proliferation based on total DNA content of human VICs on days 1, 4, 7, and 14. D) Cell metabolic activity measured by Alamar blue assay at days 1, 7, and 14 for cells cultured on scaffolds and tissue culture plates (data has been normalized to initial values for comparison).

with the properties of fibroblasts and smooth muscle cells, expressing αSMA and myosin with possible contraction.[55,59] The αSMA-positive phenotype has been observed in 50%–78% of cells isolated from intact heart valves.[59,61] This evidence has contributed to the consensus that culturing VICs on stiff 2D tissue culture polystyrene increases their activation and expression of αSMA, highlighting one of the multiple roles that substrate stiffness can play in modulating cell phenotype.

However, there has been limited research investigating the precise levels of stiffness required to induce myofibroblast activation. In a recent study, encapsulated porcine VICs in relatively stiff pure hyaluronic acid hydrogels spread more than in gels of lower stiffness. The cells also dramatically upregulated alpha smooth muscle actin expression, resembling activated myofibroblasts as gel stiffness increased.[62] The few measurements taken, have defined a substrate stiffness region of approximately 15 kPa or more for VIC activation.[63] Here, human VICs cultured on our scaffolds had slightly higher αSMA expression for less stiff material (4 MPa for (2:1) to 9 MPa for (1:4) ratio of PGS:PCL) (Figure 6B). Moreover, lower expression of αSMA was observed on the scaffolds (about 1.5-fold) as compared to cells cultured on tissue culture treated plastic (stiffness ≈ 3 GPa).[64] Interestingly, we observed no changes in αSMA expression over time, similar to native valvular cells that remain quiescent and fibroblast-like (Figure 6B). To further assay VIC phenotypic markers, cells on aligned scaffolds were immunostained for the presence of vimentin and αSMA proteins (**Figure 7**A,B). Immunostaining was also performed for vimentin on the random fibers, which indicated no significant differences (Supporting Information, Figure 2A).

Cell Proliferation and Metabolic Activity. Cell proliferation and metabolic activity were assayed on the different ratios of PGS:PCL scaffolds to evaluate the effect of substrate stiffness. The results showed that human VICs exhibited significantly enhanced proliferation and metabolic activity, about three-fold and two-fold, respectively, following 14 days of culture compared to days 1 and 7 (Figure 6C,D). Contrary to what was observed with porcine cells (Supporting Information, Figures 3E–F), human cells had a slower rate of proliferation and lower metabolic activity in the initial week of culture. The human cells also required more time to initially adapt to their environment before regular proliferation commenced. There was no considerable difference in cell proliferation between each ratio of the PGS:PCL scaffolds as expected and this is likely due to the presence of PGS in the composite. Previously, it has been shown that any combinations of PGS:PCL scaffolds have higher cellular metabolic activity than pure PCL scaffolds.[13] Here, the cultured cells on scaffolds were shown to have a favorable tolerance of each of the PGS:PCL ratios tested.

2.3. Porcine VICs Response to PGS:PCL Scaffolds

Supporting Information, Figure 3 is composed of the data with porcine VICs cultured on PGS:PCL scaffolds for 10 d. At day 1, cell spreading was greater on the less stiff (less PCL content) constructs (Supporting Information, Figure 3A), as demonstrated for the (2:1) and (1:4) ratios. This difference was also observed for the human VICs, wherein the cells were spread more at day 1 on less stiff scaffolds (Supporting Information, Figure 2B). These analyses were made by staining the cells on the scaffolds with F-actin. We did not observe large changes in cell spreading over time on scaffolds (Supporting Information, Figure 3B).

Cell attachment, viability, proliferation, and metabolic activity were also assessed for the porcine cells seeded on scaffolds with different PGS and PCL ratios. Similar to the human VICs, the results showed no significant differences in porcine cell behavior when cultured on scaffolds with varying polymer ratios. Cell attachment was slightly higher for the porcine VICs (about 85% of the initial cell seeding density) when compared

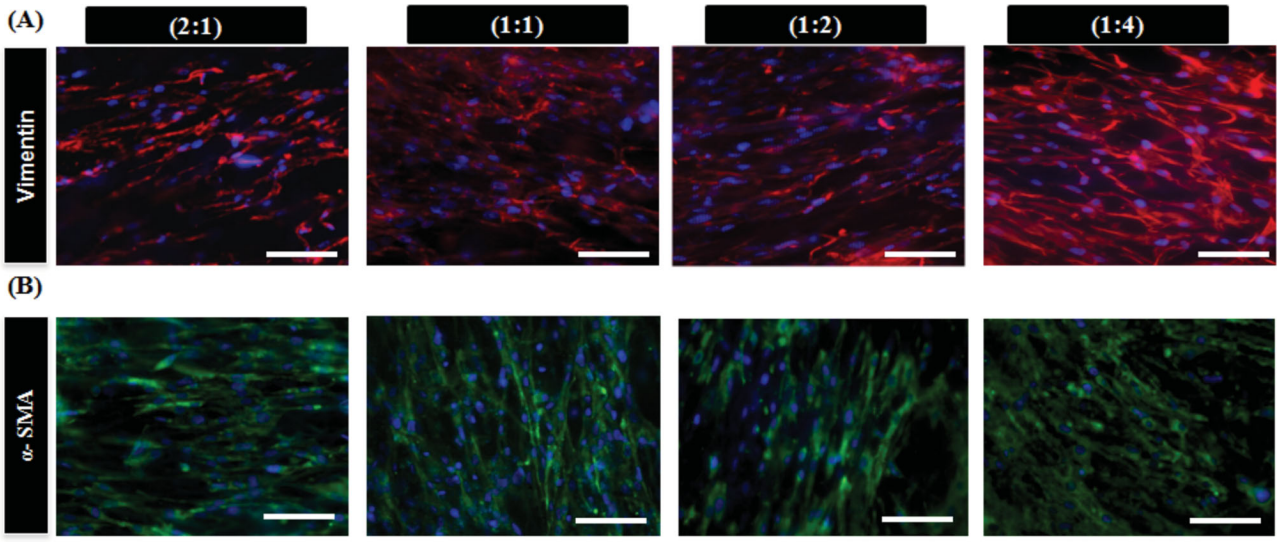

Figure 7. The effect of aligned scaffolds on vimentin and αSMA expression. A,B) Representative fluorescence images of human VICs immunostained for A) vimentin (red), and DAPI (blue), and B) αSMA (green) on the aligned scaffolds at day 14 (scale bar = 100 μm).

with human VICs (Supporting Information, Figure 3C). Cell viability measurements confirmed similar results where slightly higher viability were observed for porcine cells but no considerable differences between the ratios, as was observed for human VICs (Supporting Information Figure 3D). Human VICs differed in their time needed to acclimate to the polymers. Freshly seeded human VICs initially underwent a stationary/lag phase, whereas porcine VICs began proliferation and had metabolic activity as soon as 3 days after seeding (Supporting Information, Figure 3E,F).

3. Conclusion

Here, we developed microfibrous PGS:PCL scaffolds, including random and aligned fibers, to support human VIC engraftment and maintenance in vitro. The mechanical properties and anisotropic characteristics of fabricated scaffolds were related to the ratio of PGS:PCL content in the scaffolds. Both human and porcine VICs were successfully cultivated for approximately 2 weeks to evaluate the cellular behavior on the fabricated composites. We demonstrated that scaffold structure affected the cellular arrangement considerably, whereas the substrate stiffness (in the range of 4–9 MPa) had minimal effects on the cell alignment. VIC attachment, viability, and proliferation followed similar trends for each polymer ratio while there was a considerable difference between the results obtained with human and porcine cells. Scaffolds with a (2:1) ratio of PGS:PCL expressed higher levels of collagen I, while αSMA expression was slightly higher for less stiff scaffolds. Interestingly, αSMA expression on scaffolds was considerably lower than those in plated cells, which indicated the ability of the scaffolds to maintain the cells in a more quiescent condition similar to native tissues. The engineered fibrous PGS:PCL scaffolds with tunable mechanical properties and architecture would potentially be suitable for the regeneration of heart valves.

4. Experimental Section

Fabrication of PGS:PCL Scaffolds Containing Aligned and Random Fibers: PGS pre-polymer was synthesized based on previously reported processes ($\bar{M}_w$ = 10 000).[21,65] Briefly, sebacic acid and glycerol with 1:1 molar ratio were reacted at 120 °C under high vacuum (≈50 mTorr) for 24 h to synthesize PGS pre-polymer. Various ratios of PGS and PCL blends (e.g., 1:4, 1:2, 1:1, and 2:1) were then dissolved in an anhydrous chloroform:ethanol (9:1) solution with the overall polymer concentration of 20% (w/v). To obtain a homogeneous mixture, the polymer solutions were allowed to mix overnight at room temperature prior to the electrospinning process.

A typical electrospinning system was employed to spin the pre-polymers into sheets (Figure 1A). The pre-polymer mixture was pushed via syringe pump at a flow rate of 2 mL h^{-1} and electrospun at 18 kV. The distance from the tip of the gauge needle to the collector plates was set at 18 cm.[13] To form electrospun sheets with randomly distributed fibers, the fibers were spun onto a glass slide placed on a grounded metallic base. Aligned fibers were created by electrospinning the fibers between two grounded electrodes, separated by 1.5 cm. The microfibers were then desiccated in a vacuum chamber overnight before further characterizations. Importantly, hydrophilicity was improved in scaffolds by immersing them in 0.05 M NaOH (Sigma–Aldrich Co., St. Louis, MO) for 5 min followed by copious washing step with PBS.

Physical Characterization of Microfibrous Scaffolds: The chemical compositions of the PGS:PCL scaffolds were evaluated by performing Fourier-transform infrared spectroscopy (FTIR) analysis (Bomem, MB 100) over a range of 500–4000 cm^{-1} and resolution of 2 cm^{-1}. In addition, the wettability of the composite scaffolds was tested by using contact angle measurement with static drop technique (video contact angle system, VCA Optima, AST Inc.).[13] Prior to obtaining scanning electron microscopy (SEM) images, the samples were sputter-coated by a thin layer of gold and palladium. The fiber diameters and pore sizes for both aligned and random scaffolds were measured by importing the related SEM images into Image J software (NIH).

In vitro degradation rate was assessed based on the weight loss of the scaffolds, measured for 10 days in 5 mL Dulbecco's phosphate buffered saline (DPBS) (GIBCO) with 0.5×10^{-3} M sodium hydroxide (NaOH) at 37 °C. Four PGS:PCL samples with a 5-mm diameter and thickness of 150 μm were cut with a biopsy punch and were used to determine the degradation rate. The scaffolds were then rinsed in DPBS and dried following each time points. The samples' weights were then measured and the percentage of mass loss was calculated by dividing the weight loss to the initial dry weight for each sample.

The tensile properties of samples with aligned and random fibers were tested under uniaxial tension using a mechanical tester (Model 5542; Instron, Norwood, MA) with 10 N load capacity and at a constant rate of 7 mm min^{-1}. The data were processed using Blue Hill software (Instron), which measured the force/deformation and stress–strain curves for each sample. Rectangular samples with a length of 10 mm, width of 5 mm, and a thickness of 0.1 mm were stretched in both dry and wet conditions for comparison. We calculated the effective stiffness of the scaffolds from the initial 0%–15% strain region of stress–stain curves (the slope E, is corresponding to Young's modulus defined for elastic homogeneous materials). The ultimate tensile strength (UTS), the maximum stress, and strain to failure (ef) were also obtained from the stress–strain curves. The mean and standard deviation values of 4–6 independent measurements were reported and considered for comparison. For structures with aligned fibers, the samples were tested in two directions; one aligned with the fiber's direction, referred to as the preferred direction (PD) and the other one perpendicular to the fiber alignment, referred to as the cross-preferred direction (XD). The anisotropic mechanical characteristics of the aligned fibers for each ratio were also calculated by dividing the average value in the PD direction by the XD direction.

VIC Isolation and Characterization: In this study, we cultured both human and porcine VICs on our microfibrous electrospun sheets. All cell culture supplies were purchased from Invitrogen (CA, USA). Human aortic VICs were obtained from the Department of Cardiac Surgery at Boston's Children Hospital. Aortic VICs were isolated from fresh aortic valve leaflets excised under sterile conditions from transplant recipients' explanted hearts with normal valve leaflets. Leaflets were washed several times in cold PBS before the endothelium was scraped off and the remaining tissue was minced with a blade to facilitate matrix digestion. It was then incubated at 37 °C for 1 h in a digestion buffer containing 10× calcium/magnesium buffer, 0.2% (v/v) type I collagenase (Roche), and 2.5 U mL^{-1} dispase (BD Bioscience) in culture medium containing Dulbecco's modified Eagle medium (DMEM), 10% fetal bovine serum (FBS), and 1% (v/v) antibiotic–antimycotic (Invitrogen). The digested tissue solution was then centrifuged at 1200 rpm for 5 min, resuspended in culture medium, and plated on tissue culture plastic. Isolated VICs were expanded and utilized between passage 3 and passage 7.

Porcine VICs were also isolated by collagenase digestion[46] from AV porcine leaflets, which were aseptically removed from donated hearts (Children's Hospital, Boston, MA). The valvular endothelial cells were first removed by wiping the leaflet surface. The tissue was then digested by using 0.5% (w/v) type I collagenase in Hank's balanced salt solution (HBSS) at 37 °C for 6–8 h. The solution containing cells was centrifuged at 1200 rpm for 10 min and the isolated porcine VICs were expanded and utilized between passages 6 and 7.

Cell Seeding: PGS:PCL scaffolds with 5 mm diameter and 100 μm thickness were used for cell seeding. The samples were soaked in 70% ethanol for 30 min followed by high-intensity UV exposure (800 mW) for 2 min. Prior to cell seeding, the scaffolds were soaked in DMEM media overnight. Each scaffold was seeded with 50 000 cells suspended in 20 μL of DMEM. The plates were incubated for 3 h initially to allow cells to attach the scaffold surface and then 200 μL media were added to each well. The media was then changed every other day.

Cell Attachment: The cell attachment to the scaffolds was quantified by counting the number of the cells adhered to the scaffolds at 12 h post-seeding. Nuclei were stained with 4,6-diamidino-2-phenylindole (DAPI, Invitrogen) for visualization. Twelve hours after the initial cell seeding, three scaffolds from each ratio of PGS:PCL were washed twice with DPBS, fixed in 4% paraformaldehyde (PF) solution in DPBS for 20 min at room temperature, and stained with DAPI. Fluorescent images were then taken from 10 regions of each scaffold surface using an inverted microscope (Nikon TE 2000-U; Nikon instruments Inc., USA). The images were analyzed by Image J software to count the number of cells per unit area.

Viability Assay: Cell viability was determined at days 1 and 10 using live/dead assay kit (calcein-AM/ethidium Bromide homodimer; Invitrogen) according to the manufacturer's protocol. Three scaffolds from each composition were washed with PBS and incubated in live/dead solution for 20 min. Fluorescent images were then taken by using an inverted fluorescence microscope (Nikon TE 2000-U; Nikon instruments Inc.) and imported into Image J software. The cell viability was calculated by dividing the number of dead cells by the total number of cells present.

Proliferation and Metabolic Activity: DNA quantification was performed to analyze the cell proliferation as described elsewhere.[6,21] Briefly, DNA content on each scaffold was measured using the PicoGreen dsDNA quantitation kit (Invitrogen) at days 1, 7, and 14. The scaffolds (n = 3 per group) were treated overnight at 60 °C with 1 mL of DNA extraction solution (papain, Na_2HPO_4, and EDTA (Sigma-Aldrich). PicoGreen solution was then added to all samples and standards and incubated at room temperature for 10 min. The absorbance was measured at 485 nm with a spectra max Gemini XS plate reader (Molecular Devices, Sunnyvale, CA) and the values were normalized to values taken from samples at day 1.

The metabolic activity of cells cultured on the scaffolds (n = 4 per group) and well-plates as a control (n = 3) were determined using the Alamar Blue (AB) assay (Invitrogen) according to the manufacturer's protocol. Briefly, AB solution in DMEM at the ratio of 1:9 was added to each scaffolds and incubated for 4 h. Two hundred microliters of the AB solutions was then transferred to a 96-well plate in duplicate and the fluorescence was determined at an excitation/emission of 550/580 nm. During the incubation time, the viable cells metabolize the resazurin dye (blue) in AB solution to resorufin (pink). The measured values were normalized to values taken from samples at day 1.

Cell Cytoskeletal Organization: Immunostaining was performed on cell-seeded scaffolds with aligned and random fibers to evaluate the cytoskeletal structure (F-actin) on day 14 of culture. After washing the samples in DPBS, the samples were fixed in 4% paraformaldehyde (PF) for 10 min at room temperature. The scaffolds were then soaked in 0.1% Triton X-100 in DPBS solution for half an hour to pearmeabilize the cells. Scaffolds were then blocked in 1% bovine serum albumin (BSA) for 1 h. F-actin staining was then performed using a 1/400 dilution of Alexa Fluor-594 phalloidin (Invitrogen) in 0.1% BSA. The cell nuclei were stained with DAPI, present in the mounting medium, added just before cover slipping.

Cell Alignment Analysis: We quantified the alignment of cells on aligned and random scaffolds by analyzing the shape of cell nuclei (stained with DAPI) on fluorescence images taken from nine different locations on each scaffold. The shape of each nucleus was fitted to elliptical geometries in Image J software. The alignment angle was defined as the major elliptical axis with respect to the horizontal axis. The normalized alignment angles were grouped in 10° increments to compare the nuclei alignments within each aligned and random fiber condition.

αSMA and Vimentin Expression: The expression of αSMA and Vimentin was visualized by immunostaining at day 14 of culture. The scaffolds were fixed with ice-cold methanol, rinsed, and incubated for one 1 h with primary antibodies for mouse anti-human αSMA (1:2000) (Sigma–Aldrich), or rabbit polyclonal anti-vimentin antibody (1:2000) (Abcam, Cambridge, MA) in 1% BSA in PBS. Scaffolds were then rinsed three times in DPBS, and incubated for 1 h in species-specific fluorescein isothiocyanate (FITC) or Texas Red-conjugated secondary antibodies (1:300) (FITC or Texas Red anti-mouse IgG (Vector Laboratories, Burlingame, CA) in 1% BSA/DPBS. The cell nuclei were stained with DAPI, present in the mounting medium, added just before cover slipping.

PCR Analysis: RNA was extracted using an RNeasy Mini Kit (Qiagen, Valencia, CA). cDNA synthesis was performed with an iScript cDNA Synthesis Kit (Bio-Rad Laboratories, Hercules, CA). DNAse I (Invitrogen) digestion of RNA samples (0.5 μg) was performed prior to reverse transcription.

GAPDH
Forward: 5′ AGCCACATCGCTCAGACAC′3
Reverse: 5′GCCCAATACGACCAAATCC′3
COL1A1:
Forward: 5′CCAAGAGGAGGGCCAAGAAGAAGG′3
Reverse: 5′GGGGCAGACGGGGCACACTC′3
αSMA
Forward: 5′TATCAGGGGGCACCACTATG′3
Reverse: 5′AGGAGCAGGAAAGTGTTTTAGA′3

All reactions were performed using Fast Star SYBR Green PCR Master Mix, at the default setting on an ABI Biosystems Step One Plus Real-Time PCR Machine with the following temperature profiles: denature at 95 °C for 10 min, and 40 cycles of 95 °C for 15 s, and 60 °C for 1 min.

Statistical Analysis: One-way ANOVA analysis was performed, followed by Tukey's multiple comparison for statistical analysis in GraphPad, Prism Software (V.5). Data reported as mean ± standard deviation (SD). for *: $P < 0.05$, **, $P < 0.01$ and ***: $P < 0.001$.

Supporting Information

Supporting Information is available from the Wiley Online Library or from the author.

Acknowledgements

The authors acknowledge funding from the National Science Foundation Career Award (DMR 0847287), the office of Naval Research Young National Investigator Award, and the National Institutes of Health (HL092836, DE019024, EB012597, AR057837, DE021468, HL099073). N.M. acknowledges the PSU bioengineering department's graduate scholarship. N.A. acknowledges the supports from The National Health and Medical Council. The authors would like to thank Joanna Kinney for her help with cell culture experiments.

Received: September 12, 2013
Revised: October 9, 2013
Published online: January 22, 2014

[1] M. S. Sacks, F. J. Schoen, J. E. Mayer, *Annu. Rev. Biomed. Eng.* **2009**, *11*, 289.
[2] M. Sewell-Loftin, Y. W. Chun, A. Khademhosseini, W. D. Merryman, *J. Cardiovasc. Transl. Res.* **2011**, *4*, 658.

[3] E. Filova, F. Straka, T. Mirejovský, J. Mašín, L. Bačáková, *Physiol. Res.* **2009**, *58*, S141.
[4] S. Neuenschwander, S. P. Hoerstrup, *Transplant Immunol.* **2004**, *12*, 359.
[5] F. J. Schoen, R. J. Levy, *J. Biomed. Mater. Res.* **1999**, *47*, 439.
[6] N. Masoumi, K. L. Johnson, M. C. Howell, G. C. Engelmayr Jr., *Acta Biomater.* **2013**, *9*, 5974.
[7] J. A. Stella, M. S. Sacks, *J. Biomech. Eng.* **2007**, *129*, 757.
[8] S. H. Alavi, V. Ruiz, T. Krasieva, E. L. Botvinick, A. Kheradvar, *Ann. Biomed. Eng.* **2013**, *41*, 547.
[9] K. S. Kunzelman, R. P. Cochran, S. S. Murphree, W. S. Ring, E. D. Verrier, R. C. Eberhart, *J. Heart Valve Dis.* **1993**, *2*, 236.
[10] S. Brody, A. Pandit, *J. Biomed. Mater. Res. Part B, Appl. Biomater.* **2007**, *83*, 16.
[11] M. S. Sacks, A. P. Yoganathan, *Philos. Trans. R. B Biol. Sci.* **2007**, *362*, 1369.
[12] S. Sant, D. Iyer, A. Gaharwar, A. Patel, A. Khademhosseini, *Acta Biomater.* **2012**, *9*, 5963.
[13] S. Sant, C. M. Hwang, S. H. Lee, A. Khademhosseini, *J. Tissue Eng. Regen. Med.* **2011**, *5*, 283.
[14] G. C. Engelmayr Jr., M. S. Sacks, *J. Biomech. Eng.* **2006**, *128*, 610.
[15] G. C. Engelmayr Jr., M. S. Sacks, *Biomech. Modeling Mechanobiol.* **2008**, *7*, 309.
[16] A. Mol, C. V. Bouten, G. Zund, C. I. Gunter, J. F. Visjager, M. I. Turina, F. P. Baaijens, S. P. Hoerstrup, *Thorac. Cardiovasc. Surgeon* **2003**, *51*, 78.
[17] P. S. Robinson, S. L. Johnson, M. C. Evans, V. H. Barocas, R. T. Tranquillo, *Tissue Eng. Part A* **2008**, *14*, 83.
[18] C. Williams, S. L. Johnson, P. S. Robinson, R. T. Tranquillo, *Tissue Eng.* **2006**, *12*, 1489.
[19] J. A. Benton, C. A. DeForest, V. Vivekanandan, K. S. Anseth, *Tissue Eng. Part A* **2009**, *15*, 3221.
[20] L. Hockaday, K. Kang, N. Colangelo, P. Cheung, B. Duan, E. Malone, J. Wu, L. Girardi, L. Bonassar, H. Lipson, *Biofabrication* **2012**, *4*, 035005.
[21] N. Masoumi, A. Jean, J. T. Zugates, K. L. Johnson, G. C. Engelmayr Jr., *J. Biomed. Mater. Res. Part A* **2013**, *101*, 104.
[22] D. Gottlieb, T. Kunal, S. Emani, E. Aikawa, D. W. Brown, A. J. Powell, A. Nedder, G. C. Engelmayr Jr., J. M. Melero-Martin, M. S. Sacks, J. E. Mayer Jr., *J. Thorac. Cardiovasc. Surg.* **2010**, *139*, 723.
[23] S. P. Hoerstrup, R. Sodian, S. Daebritz, J. Wang, E. A. Bacha, D. P. Martin, A. M. Moran, K. J. Guleserian, J. S. Sperling, S. Kaushal, *Circulation* **2000**, *102*, 44.
[24] P. W. Riem Vis, J. Kluin, J. P. Sluijter, L. A. van Herwerden, C. V. Bouten, *Eur. J. Cardio-Thorac. Surgery: Official J. Eur. Assoc. Cardio-Thorac. Surg.* **2011**, *39*, 8.
[25] M. S. Sacks, W. D. Merryman, D. E. Schmidt, *J. Biomech.* **2009**, *42*, 1804.
[26] J. L. Ifkovits, J. J. Devlin, G. Eng, T. P. Martens, G. Vunjak-Novakovic, J. A. Burdick, *ACS Appl. Mater. Interfaces* **2009, 1**, 1878.
[27] J. L. Ifkovits, R. F. Padera, J. A. Burdick, *Biomed. Mater.* **2008**, *3*, 034104.
[28] F. Yi, D. A. LaVan, *Macromol. Biosci.* **2008**, *8*, 803.
[29] S. Catledge, W. Clem, N. Shrikishen, S. Chowdhury, A. Stanishevsky, M. Koopman, Y. Vohra, *Biomed. Mater.* **2007**, *2*, 142.
[30] W. Cai, L. Liu, *Mater. Lett.* **2008**, *62*, 2171.
[31] Z.-J. Sun, C. Chen, M.-Z. Sun, C.-H. Ai, X.-L. Lu, Y.-F. Zheng, B.-F. Yang, D.-L. Dong, *Biomaterials* **2009**, *30*, 5209.
[32] N. Annabi, J. W. Nichol, X. Zhong, C. Ji, S. Koshy, A. Khademhosseini, F. Dehghani, *Tissue Eng. Part B, Rev.* **2010**, *16*, 371.
[33] A. Annabi, A. Tamayol, J. A. Uquillas, M. Akbari, L. E. Bertassoni, C. Cha, G. Camci-Unal, M. R. Dokmeci, N. A. Peppas, A. Khademhosseini, *Adv. Mater.* **2013**, DOI: 10.1002/adma.201303233.
[34] S. Kumbar, R. James, S. Nukavarapu, C. Laurencin, *Biomed. Mater.* **2008**, *3*, 034002.
[35] C. X. Lam, M. M. Savalani, S.-H. Teoh, D. W. Hutmacher, *Biomed. Mater.* **2008**, *3*, 034108.
[36] C. A. Sundback, J. Y. Shyu, Y. Wang, W. C. Faquin, R. S. Langer, J. P. Vacanti, T. A. Hadlock, *Biomaterials* **2005**, *26*, 5454.
[37] Y. Wang, Y. M. Kim, R. Langer, *J. Biomed. Mater. Res. Part A* **2003**, *66*, 192.
[38] Y. Zhang, J. Venugopal, Z.-M. Huang, C. Lim, S. Ramakrishna, *Polymer* **2006**, *47*, 2911.
[39] J.-W. Lu, Z.-P. Zhang, X.-Z. Ren, Y.-Z. Chen, Y. JIAN, Z.-X. Guo, *Macromolecules* **2008**, *41*, 3762.
[40] R. A. Rippel, H. Ghanbari, A. M. Seifalian, *World J. Surg.* **2012**, *36*, 1581.
[41] J. L. Berry, J. A. Steen, J. K. Williams, J. E. Jordan, A. Atala, J. J. Yoo, *Ann. Biomed. Eng.* **2010**, *38*, 3272.
[42] W. D. Merryman, J. Liao, A. Parekh, J. E. Candiello, H. Lin, M. S. Sacks, *Tissue Eng.* **2007**, *13*, 2281.
[43] I. El-Hamamsy, K. Balachandran, M. H. Yacoub, L. M. Stevens, P. Sarathchandra, P. M. Taylor, A. P. Yoganathan, A. H. Chester, *J. Am. College Cardiol.* **2009**, *53*, 1448.
[44] W. D. Merryman, H. Y. Huang, F. J. Schoen, M. S. Sacks, *J. Biomech.* **2006**, *39*, 88.
[45] D. E. Discher, P. Janmey, Y.-l. Wang, *Science* **2005**, *310*, 1139.
[46] W. D. Merryman, I. Youn, H. D. Lukoff, P. M. Krueger, F. Guilak, R. A. Hopkins, M. S. Sacks, *Am. J. Physiol. Heart Circ. Physiol.* **2006**, *290*, H224.
[47] A. Lewinsohn, A. Anssari-Benham, D. Lee, P. Taylor, A. Chester, M. Yacoub, H. Screen, *Proc. Inst Mech. Eng. H: J. Eng. Med.* **2011**, *225*, 821.
[48] C. Hwang, Y. Park, J. Park, K. Lee, K. Sun, A. Khademhosseini, S. Lee, *Biomed. Microdevices* **2009**, *11*, 739.
[49] M. Nikkhah, N. Eshak, P. Zorlutuna, N. Annabi, M. Castello, K. Kim, A. Dolatshahi-Pirouz, F. Edalat, H. Bae, Y. Yang, *Biomaterials*, **2012**, *33*, 9009.
[50] D. Kai, M. P. Prabhakaran, G. Jin, S. Ramakrishna, *J. Biomed. Mater. Res. Part B: Appl. Biomater.* **2011**, *98*, 379.
[51] I. C. Parrag, P. W. Zandstra, K. A. Woodhouse, *Biotechnol. Bioeng.* **2011**, *109*, 813.
[52] N. Annabi, K. Tsang, S. M. Mithieux, M. Nikkhah, A. Ameri, A. Khademhosseini, A. S. Weiss, *Adv. Funct. Mater.* **2013**, *23*, 4950.
[53] M. Kharaziha, M. Nikkhah, S. R. Shin, N. Annabi, N. Masoumi, A. K. Gaharwar, G. Camci-Unal, A. Khademhosseini, *Biomaterials* **2013**, *34*, 6355.
[54] S. Miyamoto, R. Iwamoto, A. Furuya, K. Takahashi, Y. Sasaki, H. Ando, F. Yotsumoto, T. Yoneda, M. Hamaoka, H. Yagi, T. Murakami, S. Hori, K. Shitara, E. Mekada, *Clin. Cancer Res.* **2011**, *17*, 6733.
[55] P. M. Taylor, P. Batten, N. J. Brand, P. S. Thomas, M. H. Yacoub, *Int. J. Biochem. Cell Biol.* **2003**, *35*, 113.
[56] E. Aikawa, P. Whittaker, M. Farber, K. Mendelson, R. F. Padera, M. Aikawa, F. J. Schoen, *Circulation* **2006**, *113*, 1344.
[57] A. C. Liu, V. R. Joag, A. I. Gotlieb, *Am. J. Pathol.* **2007**, *171*, 1407.
[58] S. Chakraborty, E. E. Wirrig, R. B. Hinton, W. H. Merrill, D. B. Spicer, K. E. Yutzey, *Dev. Biol.* **2010**, *347*, 167.
[59] G. A. Walker, K. S. Masters, D. N. Shah, K. S. Anseth, L. A. Leinwand, *Circ. Res.* **2004**, *95*, 253.
[60] E. Rabkin, M. Aikawa, J. R. Stone, Y. Fukumoto, P. Libby, F. J. Schoen, *Circulation* **2001**, *104*, 2525.
[61] A. H. Chester, P. M. Taylor, *Philos. Trans. R. Soc. Lond. B Biol. Sci.* **2007**, *362*, 1437.
[62] B. Duan, L. A. Hockaday, E. Kapetanovic, K. H. Kang, J. T. Butcher, *Acta Biomater.* **2013**, *9*, 7640.
[63] A. M. Kloxin, J. A. Benton, K. S. Anseth, *Biomaterials* **2010**, *31*, 1.
[64] P. Bajaj, X. Tang, T. A. Saif, R. Bashir, *J. Biomed. Mater. Res. A* **2010**, *95*, 1261.
[65] Y. Wang, G. A. Ameer, B. J. Sheppard, R. Langer, *Nat. Biotechnol.* **2002**, *20*, 602.